JOURNAL OF AIRCRAFT
Vol. 36, No. 2, March–April 1999

Hybrid-Propulsion High-Altitude Long-Endurance Remotely Piloted Vehicle

M. Harmats* and D. Weihs†
Technion—Israel Institute of Technology, Technion City, Haifa 32000, Israel

The feasibility of combining solar and internal-combustion propulsion in propeller-driven remote piloted vehicles (RPV) is considered. Solar energy, converted by photovoltaic cells, is used to drive electric motors during hours of daylight while turbocharged internal combustion engines are used during hours of darkness. The purpose of this combination is to obtain a reasonably sized vehicle (compared with a pure solar-propelled vehicle), at the expense of limiting endurance. A sizing study of the hybrid-propulsion RPV for given payload and maximal endurance was performed. Optimization of RPV aerodynamic configuration and weight distribution, propeller configuration, and cruise velocity was performed, and a novel daytime extra solar energy storage method is presented. For a 100 kg/500 W payload and required endurance of 7 days at 32° north latitude, a 1000-kg RPV, with a wingspan of 39 m was obtained. The design includes four propellers of 5 m diameter, each driven by a combination of a 4-hp electric motor and a 4-hp internal-combustion engine. Ninety percent of the top wing surface is covered by solar cells, which supply 20–40% of daily RPV requirements, depending on the time of year.

Nomenclature

A = wing aspect ratio
At = atmosphere attenuation coefficient
A_{tot} = daily total insolation in horizontal plane, W-h/m^2
A_{used} = part of A_{tot} used by the RPV during hours of daylight, W-h/m^2
b = wingspan, m
C_{D_0} = total RPV drag coefficient not including the induced drag, $(D - kC_L^2)/QS$
C_L = RPV lift coefficient, L/QS
C_L^* = C_L for maximal aerodynamic efficiency
$C_{L_{opt}}$ = C_L for minimal power climb
c = wing chord, m
E = specific energy, m
ED = energy storage density, W-h/kg
E_{save} = saved energy as a result of the combustion engines operation delay, W
E_{stor} = stored energy, W
FP = fuel part of the takeoff gross weight
Fu = RPV fuel weight, kg
f = maximal to mean power ratio (daily)
f_e = definition of specific energy derivative vs time in the RPV dynamics model, m/s
g = standard gravity acceleration, 9.80665 m/s^2
H = altitude, m or ft
Ha = Hamiltonian
h = see definition in Eq. (46)
k = induced drag factor
m = specific weight, kg/kW or kg/m^3
m_{pc} = weight per unit area of photovoltaic cells, kg/m^2
m_{pc_1} = see definition in Eq. (29), kg/m^2
N_p = number of propellers
n = sequential day number (n = 1 for January 1)
n_z = normal load factor, g
P = power, hp or W
P_{cm} = internal combustion engine daily mean power
P_{cm-max} = internal combustion engine daily maximal power
P_{em} = electric motor daily mean power
P_{em-max} = electric motor daily maximal power
P'_{pl} = daily mean extracted shaft power for the payload
P_{req} = required power for RPV level flight
P_s = propeller shaft power
P_{sol} = daily mean solar power utilized by the RPV
$P_{sol-max}$ = daily maximal $P_{sol-var}$
$P_{sol-var}$ = available solar power
Q = dynamic pressure, $0.5\rho V^2$
Re = Reynolds number
r_{pc} = solar cell area to wing area ratio
r_{str} = RPV structural fraction of gross weight
r_t = fuel tanks to fuel weight ratio
r_w = see definition in Eq. (30)
S = RPV wing area, m^2
SI_E = solar irradiance on the Earth (above the atmosphere), W/m^2
SI_{req} = solar irradiance required for a level flight, W/m^2
SI_{used} = mean solar irradiance used by the RPV during hours of daylight, W/m^2
SI_{var} = solar irradiance on a horizontal plane inside the atmosphere, W/m^2
T = cruise time, days; or temperature, deg
t = solar time (t = 12 when the sun is in zenith), h
t_{desc} = duration of a descent from maximal to cruise altitude, h
t_f = time of return to cruise altitude, h
t_l = time of light ($t_{ss} - t_{sr}$), h
t_{loft} = duration of descent from cruise to maximal altitude, h
t_{sr} = sunrise time, h
t_{ss} = sunset time, h
V = RPV velocity, m/s
V_{eq} = RPV equivalent velocity, $(V\sqrt{\rho/\rho_{sea-lev}})$
W = weight, kg
W_1 = see definition in Eq. (24)
x = solar radiation required for RPV level flight to the daily maximal radiation ratio
Y = wingspan coordinate, m
y = wingspan nondimensional coordinate, $Y/(b/2)$
z = see definition in Eq. (23), 1/day
β = angle of latitude, deg

Received Feb. 2, 1998; revision received Aug. 1, 1998; accepted for publication Aug. 4, 1998.

*M.S. in Aerospace Engineering.

†Richmond Professor of Aerospace Engineering and Provost.

γ = flight-path angle, deg
δ = Earth declination, deg
ε = RPV aerodynamic efficiency, L/D
η = efficiency
λ_e = Lagrange multiplier of the energy variable, s/m
μ = geographic latitude, deg; or air viscosity, kg-m/s
ρ = air density, kg/m^3
ρ_H = derivative of ρ with the altitude, kg/m^4

Subscripts
b = battery or fuel cell
base = at cruise base altitude
cm = internal combustion engine
eff = effective
eg = electricity generator
em = electric motor
F = at cruise end
f = back to cruise altitude
gear = transmission
max = daily maximal
mean = mean during cruise
p = propulsion (includes propeller and gear)
pc = photovoltaic cell
pl = payload
prop = propeller
ref = reference
sol = solar
str = structural
t = fuel tanks
0 = first day of cruise

Introduction

OVER the last 25 years, several studies and projects have dealt with the utilization of solar energy to keep an aerial vehicle aloft. The most promising method for doing that is by converting solar energy into electricity by photovoltaic cells, and then to use the electricity to drive propellers by means of electric motors. Such propulsion was actually realized in the following aerial vehicles that flew for up to several hours:

1) Sunrise I/II–remote piloted vehicles (RPVs) constructed in 1974–1975 by AstroFlight.[1,2]

2) Gossamer Penguin and Solar Challenger manned vehicles constructed in 1980–1981 by AeroVironment.[1–3]

3) Pathfinder–RPV constructed in 1992–1993 by AeroVironment. In 1995 it performed a demonstration flight of 12 h at an altitude of 50,000 ft. This design was based on a prototype that in 1983 performed test flights of 30–60 min at altitudes of up to 8500 ft, using AuZn batteries.[4,5]

The previously mentioned vehicles were able to fly only during daylight.

Since 1980, several studies have been performed using solar energy for keeping an RPV aloft for at least several days. Such a vehicle must have the ability to continue flying during the night and, therefore, requires electricity storage devices. In past sizing studies,[6–11] it was found that pure solar propulsion necessitates a huge wingspan (more than 100 m for a payload of 100 kg) and an enormous wing aspect ratio of more than 35. The problem with pure solar propulsion arises from the high specific weight of electric energy storage devices. This takes into consideration the possible improvements in the technology of rechargeable fuel cells (RFC) in the next decade that will enable, for 24-h cycle, a storage density of 600 W-h/kg, with a storage efficiency of 55%.

This paper deals with the option of combining solar propulsion with electric motors during daylight and internal combustion (reciprocating) engines during darkness. Both types of engine are combined in the driving of propellers (see block diagram in Fig. 1). The proposed RPV configuration is described in Fig. 2. The purpose of this combination is to make the most of the advantages of the two types of propulsion, allowing some necessary compromise, i.e., obtaining a reasonably sized aerial vehicle (compared with a pure solar propulsion vehicle), at the expense of limiting the endurance.

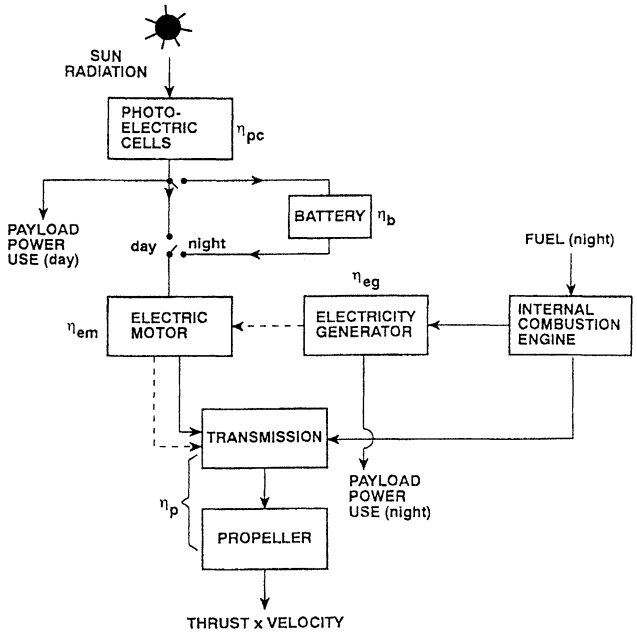

Fig. 1 Block diagram of RPV propulsion system. Dashed lines refer to the application of the electric motor as an electricity generator.

We performed a sizing procedure for a hybrid propulsion high-altitude long-endurance (HALE) RPV, with the objective of obtaining a minimal wingspan for a given payload and a given required endurance (several days). This optimization criterion was chosen because, as mentioned earlier, one of the most severe problems concerning the utilization of solar energy is the size of the RPVs, and not necessarily their gross weight. We considered two methods of joining the electric motor and the internal-combustion engine to drive the propeller. The first method is a common drive-shaft installation with a clutch that enables driving the propeller by each of the engines separately. The second possibility is to use the internal-combustion engine as an electricity generator that operates the electric motor together with the photovoltaic cells. The second method simplifies the transmission mechanics. The following three cases were considered for dealing with the extra daytime solar energy.

Case 1: Excess energy is not used, but rejected to the atmosphere.

Case 2: Excess energy is stored in a battery or an RFC and used during the hours of darkness.

Case 3: Excess energy is used for climb. When night begins, the RPV descends back to the initial altitude with nonoperating internal combustion engines.

In the third case, the fuel, otherwise required to keep a constant flight altitude during the beginning of the night, is saved. In the present paper, this climb and descent maneuver is defined as a *potential energy battery*, with 100% degree of discharge (DOD) and zero self-weight.

Sizing Equations of Hybrid-Propulsion RPV

The set of sizing equations consists of the RPV equilibrium equations (in terms of power) and of solar irradiance relations. The three possibilities of utilizing daytime extra solar energy are described in the Introduction (cases 1–3). The equations of motion describe power equilibrium for the first day of cruise, which is the most critical because of the full fuel load.

In the following days, the power requirements decrease as a result of RPV weight reduction caused by fuel consumption. For cruise at constant altitude and velocity

$$P_{\text{req}_0} = P_{\text{cm}_0} + P_{\text{sol}_0} \tag{1}$$

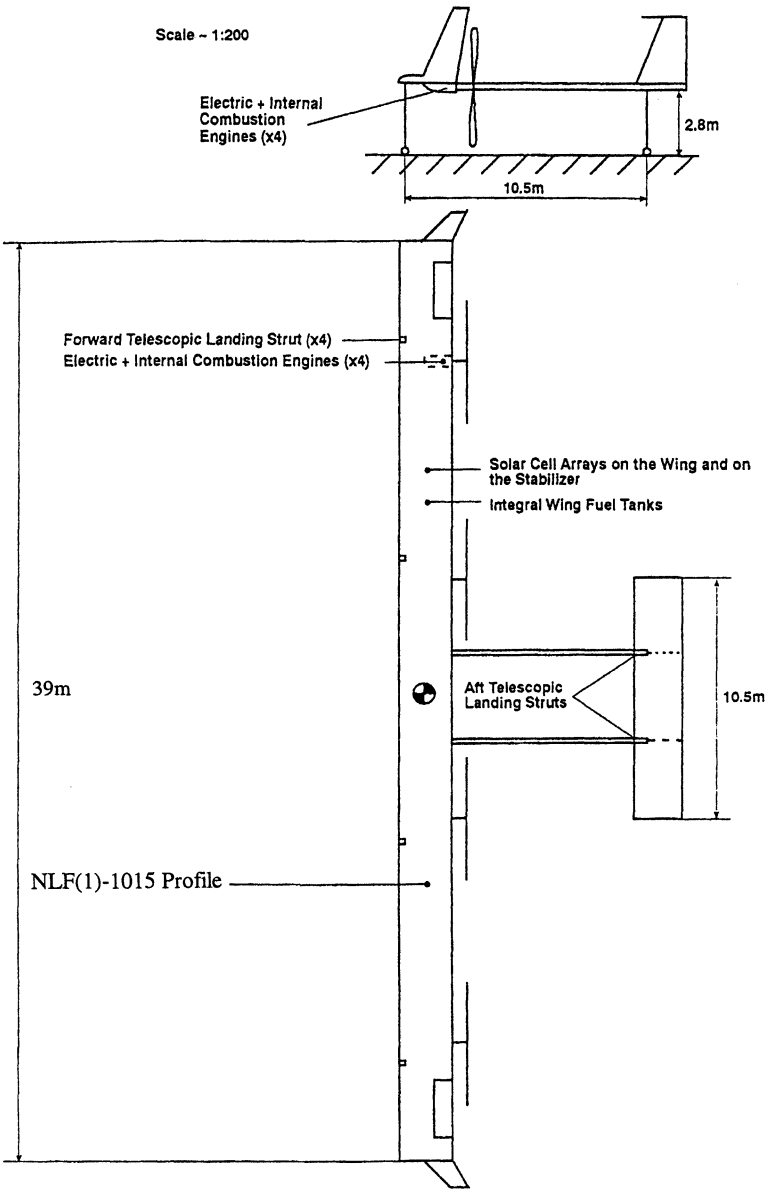

Fig. 2 Nominal RPV configuration.

$$P_{\text{req}_0} = (C_{D_0} + kC_{L_0}^2)\frac{SQV}{\eta_P} + P'_{\text{pl}} = \frac{W_0 gV}{\eta_P \varepsilon_0} + P'_{\text{pl}} \tag{2}$$

$$\varepsilon_0 = \frac{C_{L_0}}{C_{D_0} + kC_{L_0}^2} \tag{3}$$

The daily mean extracted shaft power for the payload is given by

$$P'_{\text{pl}} = P_{\text{pl}}\left(\frac{t_l}{24}\eta_{\text{em}} + \frac{24 - t_l}{24}\frac{1}{\eta_{\text{eg}}}\right) \tag{4}$$

This expression assumes that the payload power is supplied by photovoltaic cells during hours of light and by an electricity generator by night:

$$P_{\text{sol}_0} = SI_{\text{used}}(x_0)Sr_{\text{pc}}\eta_{\text{pc}}\eta_{\text{em}} \quad \text{(case 1)} \tag{5}$$

$$P_{\text{sol}_0} = \left[SI_{\text{used}}(x_0) + \frac{A_1(x_0)\eta_b}{24}\right]Sr_{\text{pc}}\eta_{\text{pc}}\eta_{\text{em}} \quad \text{(cases 2 and 3)} \tag{6}$$

$$SI_{\text{used}} = A_{\text{used}}\,24$$

In case 2, η_b is the efficiency of electric energy storage by a battery or an RFC.

In case 3, η_b is the efficiency of potential energy storage by the climb and descent maneuver.

The solar irradiance parameters A_1 and A_{used} are described in Fig. 3. The solar irradiance curve in this figure represents the irradiance in the following relation:

$$SI_{\text{var}} = SI_E At\cos(\beta - \delta)\frac{\sin\beta\sin\delta - \cos\beta\cos\delta\cos(\pi t/12)}{\cos(\pi - \delta)} \tag{7}$$

where

$$SI_E = 1353[1 + 0.033\cos(2\pi n/365)] \tag{8}$$

$$\delta = 23.45\sin[2\pi(284 + n)/365] \tag{9}$$

$$x_0 = SI_{\text{req}_0}/SI_{\max} = P_{\text{req}_0}/P_{\text{sol}-\max}$$
$$P_{\text{sol}-\max} = SI_{\max}Sr_{\text{pc}}\eta_{\text{pc}}\eta_{\text{em}} \tag{10}$$

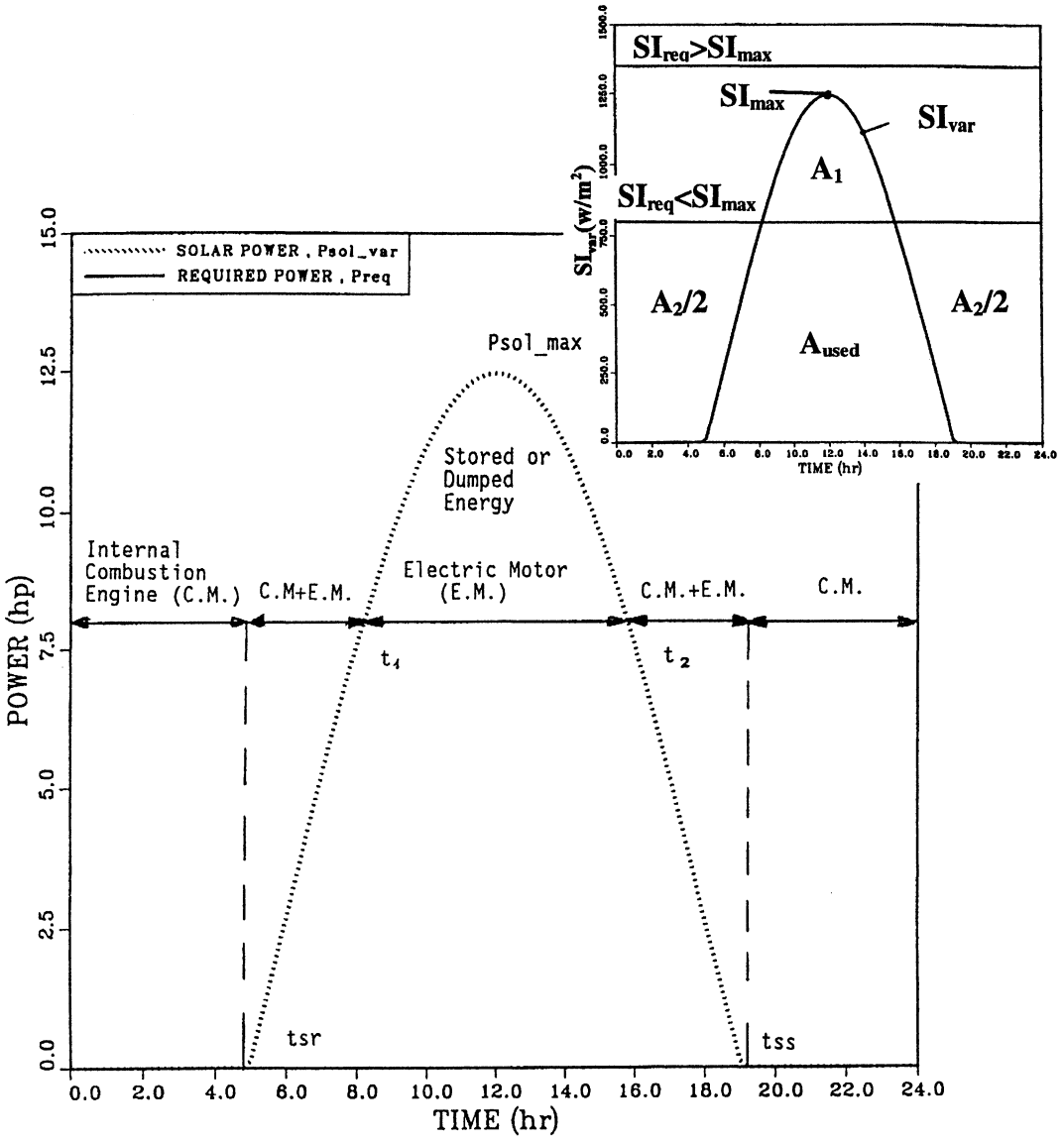

Fig. 3 Power required for cruise and available power vs time (including definition of solar irradiance parameters).

The mean output power of the engines in the first day is given by

$$P_{\mathrm{em}_0} = P_{\mathrm{sol}_0} - P_{\mathrm{pl}}(t_l/24)\eta_{\mathrm{em}} \tag{11}$$

$$P_{\mathrm{cm}_0} = P_{\mathrm{req}_0} - P_{\mathrm{sol}_0} \tag{12}$$

The maximal output power is given by

$$P_{\mathrm{cm-max}_0} = P_{\mathrm{req}_0} \tag{13}$$

$$P_{\mathrm{em-max}_0} = P_{\mathrm{req}_0} - P_{\mathrm{pl}}\eta_{\mathrm{em}} \tag{14}$$

and, in cases 1 and 2 when $P_{\mathrm{sol-var}} > P_{\mathrm{req}}$, by

$$P_{\mathrm{em-max}_0} = P_{\mathrm{sol-max}_0} - P_{\mathrm{pl}}\eta_{\mathrm{em}} \quad \text{otherwise} \tag{15}$$

The RPV initial gross weight is obtained by solving the following differential equation:

$$W = -\frac{\mathrm{SFC}V}{\varepsilon(C_L)\eta_p} \times \frac{24g}{1000} W - (P_{\mathrm{pl}} - P_{\mathrm{sol}})\mathrm{SFC}\,\frac{24}{1000} \tag{16}$$

where the specific fuel consumption (SFC) is measured in kg/(kW · h).

With the boundary conditions:

$$T = T_0, \qquad W = W_0$$

$$T = T_F, \qquad W = W_F$$

When RPV size optimization is performed, W_0 and W_F are not known in advance. An analytical solution of Eq. (16) can be obtained by using mean (over the cruise duration) values of ε and P_{sol}.[12] The mean value of P_{sol} is given by

$$P_{\mathrm{sol-mean}} = SI_{\mathrm{used-mean}} Sr_{\mathrm{pc}}\eta_{\mathrm{pc}}\eta_{\mathrm{em}} \quad \text{(case 1)} \tag{17}$$

$$P_{\mathrm{sol-mean}} = \left[SI_{\mathrm{used-mean}} + \frac{A_1(x_0)\eta_b}{24}\right] Sr_{\mathrm{pc}}\eta_{\mathrm{pc}}\eta_{\mathrm{em}} \quad \text{(case 2)} \tag{18}$$

$$P_{\mathrm{sol-mean}} = \left\{SI_{\mathrm{used-mean}} + \left[\frac{A_1(x_0)\eta_b(x_0) + A_1(x_F)\eta_b(x_F)}{48}\right]\right\} \times Sr_{\mathrm{pc}}\eta_{\mathrm{pc}}\eta_{\mathrm{em}} \quad \text{(case 3)} \tag{19}$$

$$SI_{\mathrm{used-mean}} = \frac{SI_{\mathrm{used}}(x_0) + 2S_{\mathrm{used}}[(x_0 + x_F)/2] + SI_{\mathrm{used}}(x_F)}{4} \tag{20}$$

$$x_F = x_0 \frac{W_F}{W_0} \frac{\varepsilon(C_{L_0})}{\varepsilon(C_{L_F})} \tag{21}$$

The difference between case 2 and case 3 evolves from the fact that, in case 2, the size of the storage device is determined by the excess solar energy in the first day of cruise. In the following days, excess energy increases and part of it is diffused into the environment, as in case 1. In contrast, in case 3, excess energy is stored during the entire cruise because there is no need for electrochemical storage devices.

The solution of Eq. (16) is

$$W = (W_0 - W_1)e^{-zT} + W_1 \tag{22}$$

$$z = \frac{\text{SFC}V}{\varepsilon_{\text{mean}}\eta_p} \frac{24g}{1000} \tag{23}$$

$$W_1 = \frac{(P_{\text{sol\_mean}} - P'_{\text{pl}})}{Vg} \varepsilon_{\text{mean}}\eta_p \tag{24}$$

From Eq. (22) we obtain the following expression for fuel weight:

$$Fu = (W_0 - W_1)(1 - e^{-zT_F}) \tag{25}$$

or

$$Fu = (W_F - W_1)(e^{-zT_F} - 1) \tag{26}$$

Assuming constant ε and P_{sol} results in a fuel weight error of not more than 0.5%.

The RPV initial weight is

$$W_0 = r_w[W_{\text{pl}} + r_{\text{pc}}m_{\text{pc}_1}S + f_{\text{cm}_0}P_{\text{cm}_0}(m_{\text{cm}}/1000) + (1 + r_t)Fu] \quad \text{(cases 1 and 3)} \tag{27}$$

$$W_0 = r_w[W_{\text{pl}} + r_{\text{pc}}(m_{\text{pc}_1} + m_b)S + f_{\text{cm}_0}P_{\text{cm}_0}(m_{\text{cm}}/1000) + (1 + r_t)Fu] \quad \text{(case 2)} \tag{28}$$

where

$$m_{\text{pc}_1} = m_{\text{pc}} + \frac{m_{\text{em}}}{1000} \frac{f_{\text{cm}_0}P_{\text{cm}_0}}{Sr_{\text{pc}}} \tag{29}$$

$$r_w = 1/(1 - r_{\text{str}}) \tag{30}$$

$$m_b = W_b/Sr_{\text{pc}} \tag{31}$$

$$W_b = A_1 Sr_{\text{pc}}\eta_{\text{pc}}/ED \tag{32}$$

The set of sizing equations was solved iteratively, for given required maximal endurance, after an initial guess of W_F, S, C_{L_0}, $\varepsilon_{\text{mean}}$, P_{cm_0}, x_0 (Fig. 4). In the first stage, double-loop computations were performed. The inner loop iterates for a given C_{L_0} and x_0 until a convergence of S is achieved. The outer loop iterates for a given C_{L_0} until a convergence of x_0 is achieved. In the second stage, C_{L_0} is varied (taking into consideration $C_{L_0} \leq C_{L_{\max}}$), until C_{L_0} for minimal S is found.

Climb and Descent Maneuver Optimization

The objective of this maneuver is the storage of extra daytime solar energy as potential energy. The maneuver consists of two stages. First, the vehicle climbs from the base cruise altitude (20 km) using electric motors utilizing excess solar energy, and then the RPV descends during the beginning of the night, back to the base altitude, with nonoperating internal-combustion engines (see a description of the maneuver in Fig. 5). The operation of the internal-combustion engine is delayed and reduced relative to constant level flight (t_f instead of t_2 in Fig. 5), and fuel is saved. Therefore, the goal of the maneuver optimization is to maximize t_f. This optimization was performed as a calculus-of-variations problem with final criterion minimization (Mayer formulation). This criterion is defined as $J = -t_f$.

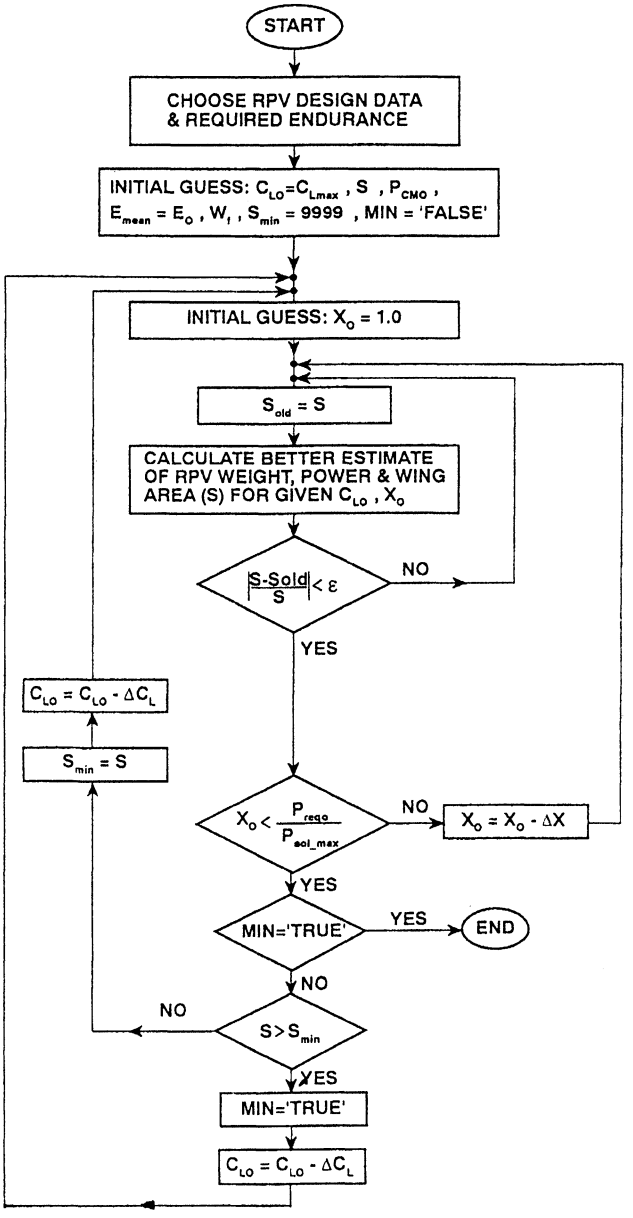

Fig. 4 Flowchart of the hybrid-propulsion RPV sizing procedure.

Differential equations of the RPV dynamics using the specific energy approximation model are (using V as the control)

$$\dot{E} = \frac{(Th - D)V}{Wg} = \frac{P_{\text{sol}}(t)\eta_p}{Wg} - \frac{(0.5\rho V^2 SC_{D_0} + 0.5\rho V^2 SkC_L^2)}{Wg} \tag{33}$$

and for $n_z = 1$ g ($C_L = Wg/0.5\rho V^2 S$):

$$\dot{E} = \frac{P_{\text{sol}}(t)\eta_p}{Wg} - \left(0.5\rho V^2 \frac{S}{Wg} C_{D_0} + \frac{2}{\rho V} \frac{W}{S} gk\right) \equiv f_e \tag{34}$$

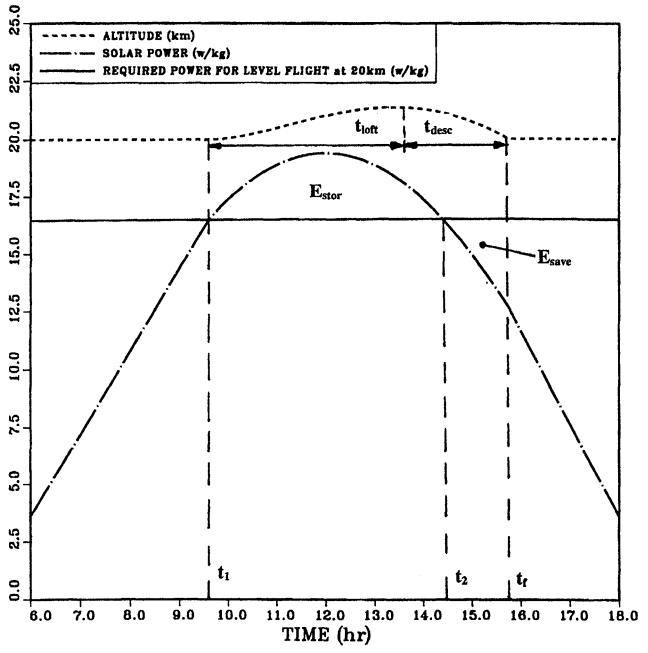

Fig. 5 Altitude and energy balance in practical climb and descent maneuver. Cruise lift coefficient = 1.07, RPV data according to Table 1, solar irradiance for summer at 32° latitude (Table 3), and ratio of (solar irradiance required for level flight at 20 km)/(maximal solar irradiance) ≡ x = 0.85.

where $P_{sol} = SI_{var}Sr_{pc}\eta_{pc}\eta_{em}$, with the boundary conditions $E(t_1) = E(t_f) = E_{base}$.

The altitude is given by

$$H = E - 0.5(V^2/g) \tag{35}$$

To find the velocity profile that minimizes J, a Hamiltonian is defined[13]:

$$Ha = \lambda_e \times f(E, V) \tag{36}$$

where f is defined by the right side of Eq. (33).

The Lagrange multiplier (λ_e) results from the simultaneous solution of Eq. (33) and

$$\dot{\lambda}_e = \frac{\partial(Ha)}{\partial E} = \lambda_e \times \frac{\partial f}{\partial V} \tag{37}$$

with unconstrained $\lambda_e(t_1)$, $\lambda_e(t_f)$, (known E_0, E_f).

The Hamiltonian at the unknown final time is given by

$$Ha(t_f) = -\frac{\partial J}{\partial t_f} \tag{38}$$

The optimality conditions are

$$\frac{\partial(Ha)}{\partial V} = 0 \tag{39}$$

$$\frac{\partial^2(Ha)}{\partial V^2} \geq 0 \quad \text{Legendre–Clebsch condition} \tag{40}$$

Implementation of Eqs. (36–40) results in

$$Ha = \lambda_e \left\{ \frac{P_{sol}\eta_p}{Wg} - \frac{0.5\rho V^3 S C_{D_0} + [2k(Wg)^2/\rho VS]}{Wg} \right\} \tag{41}$$

$$\dot{\lambda}_e = -\left. \frac{\partial f_e}{\partial \rho} \frac{d\rho}{dH} \frac{\partial H}{\partial E} \right|_v \lambda_e = \left[0.5V^3 \left(\frac{S}{W}\right) \frac{1}{g} C_{D_0} - \frac{2}{\rho^2 V} \left(\frac{W}{S}\right) gk \right] \rho_H \lambda_e \tag{42}$$

$$Ha(t_f) = 1 \tag{43}$$

$$\left.\frac{\partial(Ha)}{\partial V}\right|_E = \left.\frac{\partial(Ha)}{\partial V}\right|_H - \frac{V}{g}\left.\frac{\partial(Ha)}{\partial V}\right|_V = -\lambda_e \left[\frac{3}{2}\rho V^2 \left(\frac{S}{W}\right)\frac{1}{g} C_{D_0} \left(1 - \frac{1}{3}h\right) - \frac{2}{\rho}\frac{1}{V^2}\left(\frac{W}{S}\right) gk(1-h) \right] = 0 \tag{44}$$

$$\frac{\partial^2(Ha)}{\partial V^2} = -\lambda_e \left\{ 3\rho V \left(\frac{S}{W}\right)\frac{1}{g} C_{D_0} \left[1 - \frac{2}{3}h - \frac{1}{2}h\left(1 - \frac{1}{3}h\right)\right] + \frac{4}{\rho}\frac{1}{V^2}\left(\frac{W}{S}\right) gk \left[1 - \frac{1}{2}h(1-h)\right]\right\} \tag{45}$$

where

$$h \equiv (\rho_H/\rho)(V^2/g) \tag{46}$$

Equation (45) is obtained assuming (ρ_H/ρ) = const and $|h| \ll 1$. The assumption is exact for a constant temperature and is a good approximation for a varying temperature $T = T(H)$. For altitudes from the tropopause to 35 km, (ρ_H/ρ) takes values between (−1/6300) and (−1/6500). The optimal velocity and lift coefficient resulting from Eq. (44) are:

$$(V^*)^2 = \frac{Wg}{\rho S}\frac{2}{\sqrt{3}}\sqrt{\frac{k}{C_{D_0}}} \times \sqrt{\frac{1-h}{1-(\frac{1}{3})h}} \tag{47}$$

$$C_L = C_{L_{opt}} = \sqrt{3}\sqrt{\frac{C_{D_0}}{k}} \times \sqrt{\frac{1-(\frac{1}{3})h}{1-h}} \tag{48}$$

This velocity is slightly higher than the velocity corresponding to a constant lift coefficient, optimal for long endurance at a constant altitude, for a propeller-driven aircraft ($C_L^* = \sqrt{3}\sqrt{C_{D_0}/k}$). In the present case, the optimal lift coefficient along the trajectory of the maneuver was between 1.48 and 1.49, compared with $C_L^* = 1.5$. Along the trajectory,[12] $\lambda_e < 0$ and, therefore, $\partial^2(Ha)/\partial V^2 > 0$, and so the second optimality condition, stated in Eq. (40), is also satisfied.

The sizing program used the optimal climb and descent maneuver, developed earlier, with minor modifications to define the properties of the *potential battery*. The modification relates the existence of the maximal lift coefficient constraint and the requirement that the RPV velocity will not drop below cruise velocity:

$$C_{L_{loft}} = \min[C_{L_{opt}}, C_{L_{max}}, (Wg/0.5\rho V_{base}^2)] \tag{49}$$

As mentioned earlier, the internal-combustion engines are operated only after the RPV descends to the cruise altitude, with a constant altitude cruise. The descent may be performed before or after sunset.

The energy storage efficiency of the maneuver is given by (see Fig. 5)

$$\eta_b = E_{save}/E_{stor} \tag{50}$$

where

$$E_{stor} = 3600A_1 Sr_{pc}\eta_{pc} \tag{51}$$

$$E_{save} = \left[\frac{A_2}{2} Sr_{pc}\eta_{pc} - (24 - t_f)\frac{P_{req_{base}}}{\eta_{em}}\right] 3600, \qquad (t_f > t_{ss}) \tag{52}$$

$$E_{\text{save}} = \left\{ \frac{P_{\text{req}_{\text{base}}}}{\eta_{\text{em}}} (t_f - t_2) - [SI_{\text{int et}}(t_f) - SI_{\text{int eg}}(t_2)] Sr_{\text{pc}} \eta_{\text{pc}} \right\} 3600 \quad (t_f < t_{\text{ss}}) \quad (53)$$

$$P_{\text{req}_{\text{base}}} = Wg V_{\text{base}} / \eta_p \varepsilon_{\text{base}} \quad (54)$$

Figure 6 shows a typical case of the dependence of the maximal climb altitude and storage efficiency on the stored energy.

Propeller Optimization for High Altitude

Most of the propeller data in the open literature relates to high velocity (>100 m/s) and low-altitude flight (<7 km). The HALE RPV operates efficiently at altitudes of ~20 km at a velocity of ~40 m/s. These conditions result in Reynolds numbers of the order of 10^5, among other things. Therefore, to achieve high propulsion efficiency, propeller optimization was performed for RPV first-day cruise conditions.

The propeller calculations were performed using the algorithm described in Ref. 14, with modifications that include the following.

1) Blade profile drag coefficient dependence on Reynolds number.

2) Evaluation of propeller diameter and shaft speed that maximize the propulsion efficiency (during the propeller design stage).

3) Evaluation of a given propeller performance for varying pitch or shaft speed.

The following results correspond to the cruise design operating conditions of 20 km, 40 m/s, and 12 kW (total RPV propulsion power). The propeller design is based on two blades with an FX 60-100 profile.

As the number of propellers increases, the optimal diameter decreases, the optimal shaft speed increases, and the related maximal efficiency slightly decreases (because of the reduction in Reynolds number).

The optimal propeller efficiency vs propeller diameter for a given shaft power appears in Fig. 7, which shows that an optimal diameter that maximizes efficiency exists.

Finally, a configuration of four propellers, 5 m in diameter, was selected. The optimal setting of the propellers, under design operating conditions, was 36-deg pitch and 300 rpm shaft speed. A propeller efficiency of 91%, not including transmission losses, was achieved under these conditions.

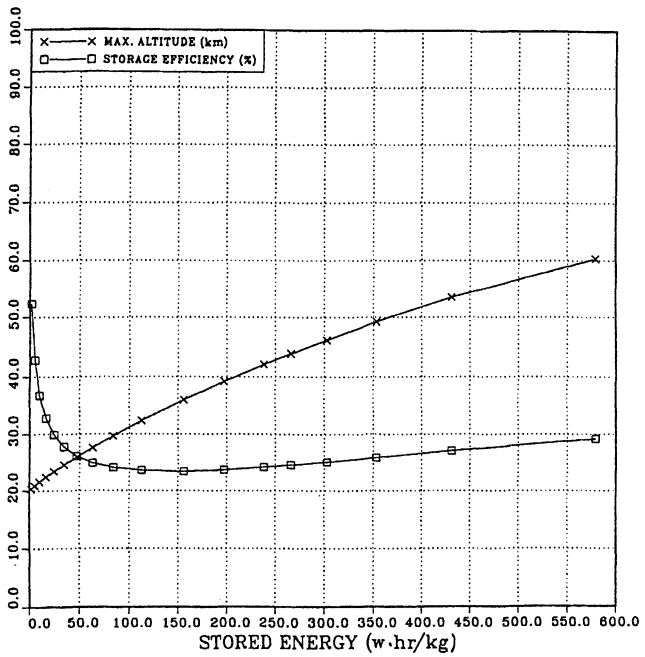

Fig. 6 Maximal altitude and storage efficiency vs stored energy per unit of RPV weight. RPV data according to Table 1; solar irradiance for summer at 32° latitude (Table 3); and altitude = 20 km, velocity = 40 m/s, shaft power = 3 kw.

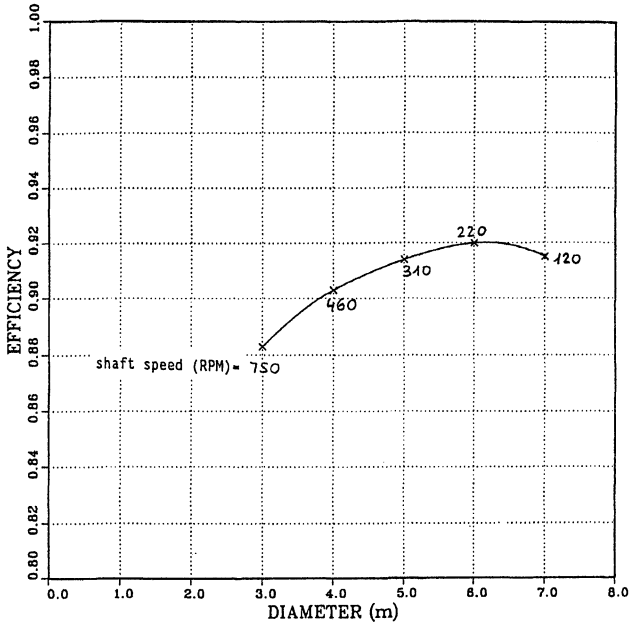

Fig. 7 Maximal propulsion efficiency vs propeller diameter.

In the second stage, an evaluation of an optimal propeller under off-design conditions was performed for the following events. A reduction of power requirement during the cruise days (event A), a high-altitude climb maneuver (event B), and a climb from sea level to the cruise altitude in the first day of the mission (event C). The performance at the off-design conditions was evaluated using two control methods: varying shaft speed for fixed pitch and varying pitch for fixed shaft speed. The conclusion is that considering the propulsion efficiency, the preferred control is by varying shaft speed with fixed pitch. This preference stands out, particularly at sea-level flight, where for a constant shaft speed, it is impossible to operate the propeller at a shaft power less than 2.5 kW. Even above this threshold the propulsion efficiency is extremely low. In event A, the optimal shaft speed slightly decreases when the shaft power decreases. In event B, the optimal shaft speed increases proportionally to shaft power; i.e., the shaft moment is kept constant.

In conclusion, it is possible to keep the propeller's efficiency above 88% in the entire RPV expected flight envelope, using a simple constant pitch propeller.

For the previously mentioned off-design conditions, the propeller speed varies between 160 and 350 rpm and the internal-combustion engine rpm is in the 1600–3000 range (50–100% of the maximal power). The engine SFC can be kept low in the whole required envelope.[27]

RPV Configuration

To assure the requirements of low wingspan and long endurance, the RPV must possess a high aerodynamic efficiency (*L/D*) for a wide range of lift coefficients and also a low structural weight fraction. The chosen aerodynamic configuration consists of a fuselageless rectangular wing with a geometric aspect ratio of 15, having tip winglets (see Fig. 2). The winglets decrease the induced drag and are most efficient for a high aspect ratio rectangular wing planform at high lift coefficient.[15] The presence of winglets is equivalent to an increase of the effective aspect ratio to 20 for the present case. We chose the NLF(1)-1015 laminar profile (laminar flow over ~50% of the wing area) with a 15% thickness ratio, designed specifically for long endurance at high altitude.[16] The RPV's tail geometry was determined in a manner that minimizes the trim drag at

Table 1 Nominal database

Parameter	Units	Value	Remarks/references
μ,	Degree	32	——
At	——	0.94	For altitude of 20 km
A	——	15	——
A_{eff}	——	20	——
C_{D_0}	——	0.015	——
$C_{L_{\max}}$	——	1.2	——
m_{em}	kg/kW	2.5	Technology of Voyager-IOL-300 turbocharged engine used in the Boeing Condor[19,25,27] (includes weight of radiators[28,29])
SFC	lb/bhp/h	0.40	Technology of Voyager-IOL-300. Covers 25–100% of the maximal engine power
	kg/kW/h	0.25	——
m_{em}	kg/kW	1	20
η_{em}	——	0.90	——
m_{pc}	kg/m^2	0.45	Crystalline silicon cell (space commerical quality)
η_{pc}	——	0.15	——
m_{prop}	kg/kW	3	6, 21
η_{prop}	——	0.90	——
m_{gear}	kg/kW	1	Mechanical transmission
η_{gear}	——	0.95	——
ED	w-h/kg	600	Hydrogen/oxygen RFC[22]
DOD	——	1	23
n_b	——	0.55	——
r_t	——	0.05	21
r_{str}	——	0.35	Derived from empty weight fraction empirical relation for home-built composite glider[12,24]

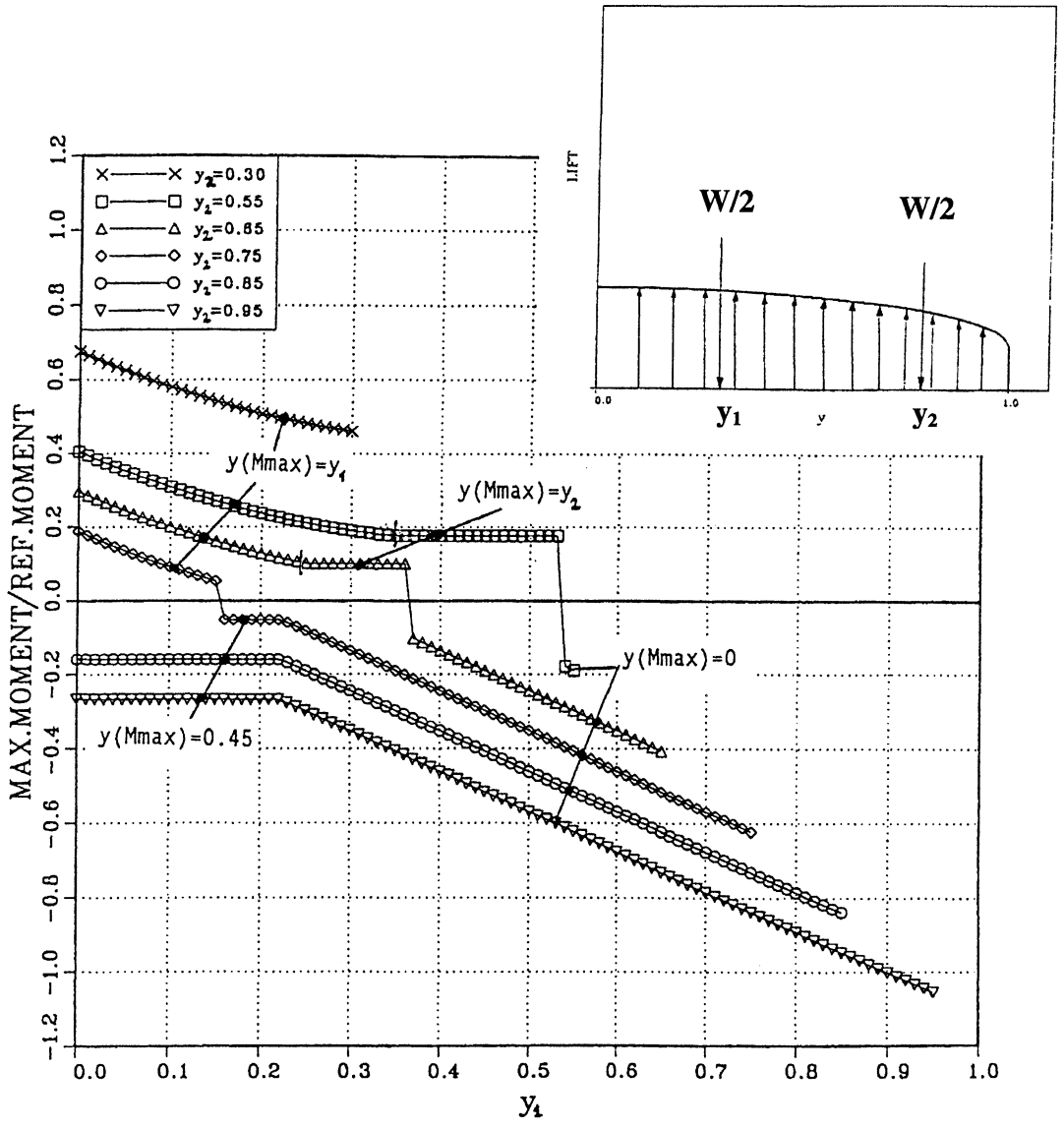

Fig. 8 Maximal bending moment along the wing caused by the installation of engines and its location vs the location of the engines. The reference moment refers to a single engine at the centerline ($y_1 = y_2 = 0$).

Table 2 Comparison of different methods of solar energy storage

Method	b_{min}, m	S_{min}, m^2	W_0, kg	W_b, kg	E_{stor}, kW-h
RFC	55	205	1700	6	4
No storage	54	195	1500	——	10 (rejected)
Climb and descent	52	180	1400	——	12

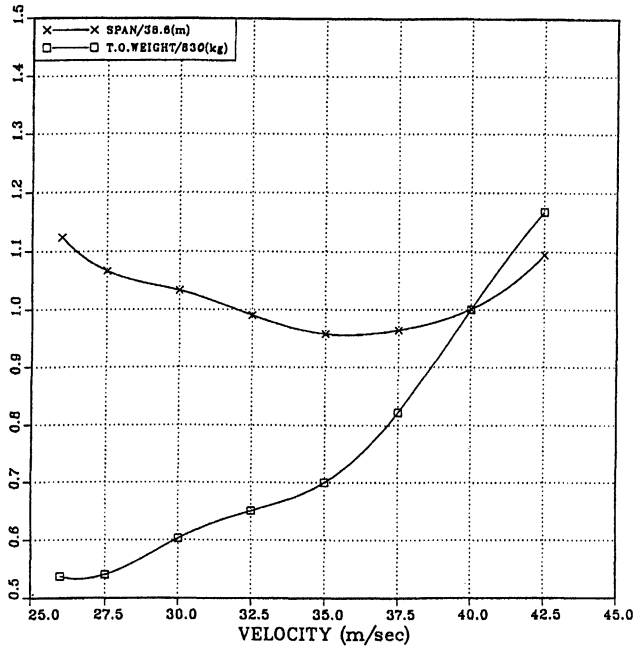

Fig. 9 Normalized minimal wingspan and takeoff weight vs cruise velocity of the RPV. The reference RPV data according to Table 1, solar irradiance for summer at 32° latitude (Table 3), and no storage of excess solar energy.

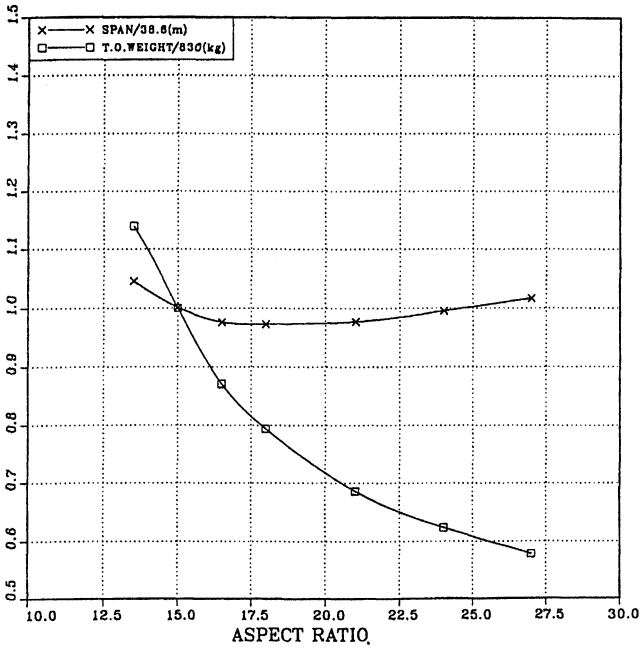

Fig. 10 Normalized minimal wingspan and takeoff weight vs geometric aspect ratio of the wing. Reference RPV data according to Table 1, solar irradiance for summer at 32° latitude (Table 3), and no storage of excess solar energy.

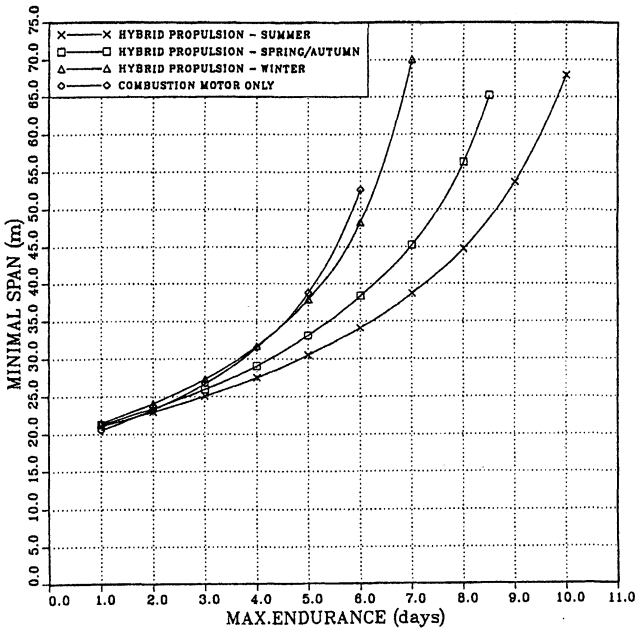

Fig. 11 Minimal wingspan vs maximal required endurance for different seasons—comparison of hybrid and pure combustion propulsion. RPV data according to Table 1, solar irradiance data according to Table 3, and each graph terminates at the maximal possible endurance for given conditions.

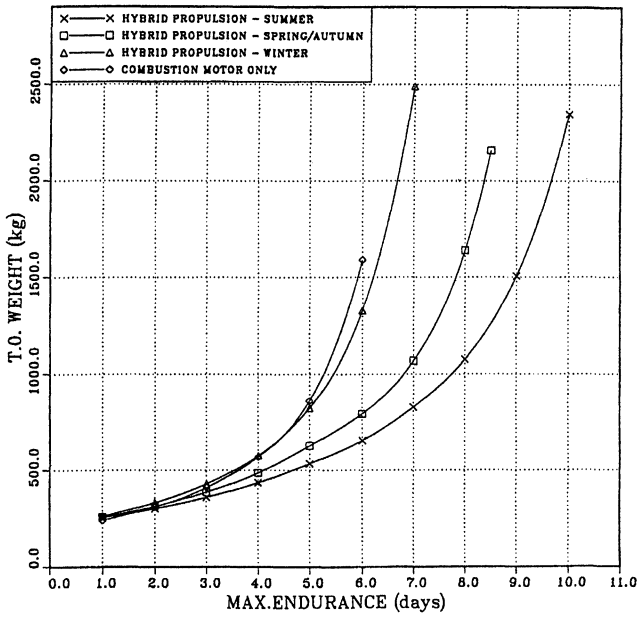

Fig. 12 RPV takeoff weight vs maximal required endurance for different seasons—comparison of hybrid and pure combustion propulsion. RPV data according to Table 1, solar irradiance data according to Table 3, and each graph terminates at the maximal possible endurance for given conditions.

nominal cruise conditions by nullification of the tail lift.[17] The estimated total coefficient of drag at zero lift is 0.015, similar to the drag of high-quality gliders. Approximately 75% of the total drag stems from the wing. Approximately 2% of the total drag is caused by the engines/radiators installation (cowling).[12] The cowling drag was estimated using the area over power ratio of the Boeing Condor,[25] by Hoerner's [26] method.

To reduce the total vehicle drag, and particularly to reduce the structural weight fraction, the design is based on distrib-

uting the vehicle's weight along the wingspan, i.e., a spanloader design.

The favorable structural effect of the spanloading arises from the bending moment reduction. The multiengine propulsion configuration facilitates the spanloading. An optimal location for four hard points that minimizes the maximal wing bending moment was obtained. The maximal bending moment and its location for different hard-point locations appears in Fig. 8. A lift distribution following the Schrenk approximation is assumed (mean of elliptical and rectangular distributions[18]). The optimization resulted in the following optimal hard-point locations: 16–22% of the wing half-span for the inner point, and 75% of the wing half-span for the outer point. This installation reduces the maximal bending moment to 5% of the reference maximal moment that results from engine centerline installation.

Reliable scaling rules for high-altitude solar RPV structural weight estimation do not exist; therefore, for this purpose, we used the most suitable data available.[6,24]

The data, as used in the RPV sizing calculations, appear in Table 1.

Sizing Results

The sizing procedure was performed for a cruise altitude of 20 km and a payload of 100 kg weight and 500 W power. For the engines we used a so-called *rubber sizing* method,[24] i.e., the input to calculations consist only of specific data that define technology (Table 1) without an a priori definition of the components' size and weight (except for the payload).

Table 3 Solar radiation data for simulations[a]

Season	Day used	t_{sr}, h	t_{ss}, h	SI_{max}, W/m^2	A_{tot}, w-h/m^2
Summer	June 22	04:57	19:03	1217	10,700
Spring/autumn	March 23	05:59	18:01	1089	8350
Winter	December 22	07:03	16:57	745	4780

[a]Sunrise and sunset hours (t_{sr}, t_{ss}) are given for solar time definition. The maximal and total insolation (SI_{max}, A_{tot}) are for At = 0.94.

Table 4 Results for minimal wingspan RPVs for required endurance of 7 days

Season	b, m	S, m^2	W_0, kg	P_{req}, hp	P_{sol}/P_{req}, %	FP, %
Summer	39	100	830	19.4	39	34
Spring/autumn	45	136	1070	24.1	34	36
Winter	70	327	2490	55.0	20	42

Different methods of extra daytime solar energy storage were compared and are presented in Table 2. The RPVs were designed for a 9-day maximum endurance during the summer.

It was concluded that it is preferable not to store the excess energy in chemical storage devices, or in very high specific energy RFC. The excess energy rejection alternative is a better alternative, and the climb and descent maneuver is the best alternative. As the maximal required endurance is reduced, the differences between the previously mentioned alternatives diminish.

The minimal RPV wingspan and the related gross weight vs cruise velocity (V) and geometric aspect ratio (A) appear in Figs. 9 and 10. We chose near-optimal values of A = 15 and V = 40 m/s (a lower velocity is problematic because of the need for stationkeeping in the presence of prevailing westerly winds). In the Mediterranean area, the wind velocity at an altitude of 20 km will exceed this velocity less than 2% of the time.[30]

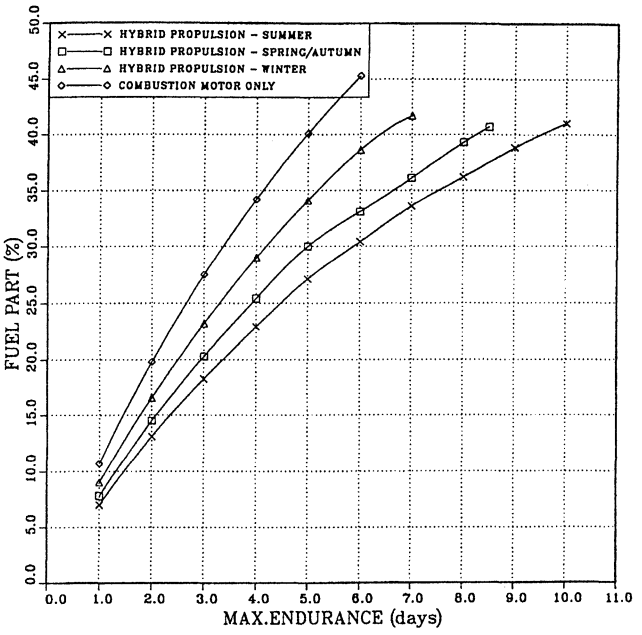

Fig. 13 Fuel fraction of takeoff weight vs maximal required endurance for different seasons — comparison of hybrid and pure internal-combustion propulsion. RPV data according to Table 1, solar irradiance data according to Table 3, and each graph terminates at the maximal possible endurance for given conditions.

Table 5 Summary of design parameter variation influence on minimal wingspan and takeoff weight of the RPV

Parameter	Δ_1, %	Δ_2, %	Δb_1, %	Δb_2, %	ΔW_1, %	ΔW_2, %
η_{em}	−5	+5	+2	−1.5	−0.5	+2.5
η_{pc}	−33[a]	+33[a]	+27	−7	+38.5	−14
η_p	−5	+5	+10	−7	+16.5	−13
SFC	−5	+5[b]	−6	+5	−12.5	+9.5
m_{em}	−50	+50[b]	−6.5	+8.5	−14	+16.5
m_{em}	−50	+50	−2.5	+3	−5.5	6
m_{pc}	−95[c]	+50	−12.5	9.5	−24.5	+19.5
m_p	−50	+50	−8	10	−16	+18
C_{D_0}	−33	+33[d]	−16.5	+37	−30	+71
r_{str}	−5	+5	−5.5	+6.5	−12	+13.5
W_{pl}	−50	+50	−24	+19.5	−44	+44
P_{pl}	−50	+50	−4	+3.5	−7	+5.5

[a]The negative increment is for an amorphous film silicon cell. The positive increment describes a GaAs or advanced silicon cell.
[b]The positive increment refers to possible characteristics deterioration following the downsizing (from 175 hp) of the reference engine.
[c]The negative increment fits amorphous thin film silicon cell.
[d]The positive increment refers to drag increase in case of turbulent flow over 100% of the wing area.

Using the internal-combustion engine as an electricity generator to drive the electric motor during hours of darkness, to simplify the transmission mechanics, was found to be ineffective because of power losses. Therefore, we chose the alternative of joining the two kinds of engines by a mechanical transmission with a clutch. In this configuration, the electric motor also serves as a starter of the internal-combustion engine.

Results for RPVs of minimal wingspan for a given required endurance from one day up to the maximal possible (technology limited) endurance appear in Figs. 11–13. For comparison, the figures include curves for different seasons and a curve for an RPV propelled solely by internal-combustion engines. Hybrid propulsion has a major effect on the maximal possible endurance increase and on the RPV size for a required long endurance. All of this is correct in summer, spring, and autumn. In winter, the hybrid propulsion RPV has no meaningful advantage over the internal-combustion engine's RPV. The solar radiation properties used in all of the calculations appear in Table 3.

Table 4 summarizes the results for the RPV's maximal required endurance of 7 days. Each of these designs can be operated under conditions different from their design conditions, taking into account that there will be a maximal endurance change. For example, an RPV that was designed for a maximal endurance of 7 days in summer is suitable for a maximal endurance of 6 days in spring or autumn, and for 5 days in winter.

The sensitivity analysis of the RPV wingspan and weight, for the design parameters' variation for the *summer* RPV in Table 4, is summarized in Table 5. The variation is relative to the nominal values in Table 1.

Acknowledgments

This paper was based in part on M. Harmats' M.S. thesis. The authors thank Scott Black, Ted Benard, and Irv Chafetz of the New England Chapter of the American Technion Society for their support. This paper was presented at the 38th Israel Annual Conference on Aerospace Sciences, Israel, February 25–26, 1998, as paper no. 11B-3.

References

[1]Boucher, R. J., "History of Solar Flight," AIAA Paper 84-1429, June 1984.

[2]Boucher, R. J., "Sunrise, the World's First Solar-Powered Airplane," *Journal of Aircraft*, Vol. 22, No. 10, 1985, pp. 840–846.

[3]MacCready, P. B., Lissaman, P. B., Morgan, W. R., and Burke, J. D., "Sun-Powered Aircraft Designs," *Journal of Aircraft*, Vol. 20, No. 6, 1983, pp. 487–493.

[4]Anon. "Fly by Night," *Flight International*, Oct. 27, 1993, pp. 36, 37.

[5]Anon. "The Eternal Airplane," *AIAA Student Journal*, Spring, AIAA, Washington, DC, 1996, pp. 2–5.

[6]Hall, D. W., Fortenbach, C. D., Dimiceli, E. V., and Parks, R. W., "A Preliminary Study of Solar Powered Aircraft and Associated Power Trains," NASA CR-3699, Dec. 1983.

[7]Youngblood, J. W., and Talay, T. A., "Solar Powered Airplane Design for Long Endurance, High Altitude Flight," AIAA Paper 82-0811, May 1982.

[8]Colozza, A. J., "Effect of Power System Technology and Mission Requirements on High Altitude, Long Endurance Aircraft," NASA CR-194455, Feb. 1994.

[9]Gilboa, Y., "Unmanned Solar Energy Propelled Vehicle," M.S. Thesis, Technion—Israel Inst. of Technology, Haifa, Israel, Dec. 1994.

[10]Brandt, S. A., and Gilliam, F. T., "Design Analysis Methodology for Solar-Powered Aircraft," *Journal of Aircraft*, Vol. 32, No. 4, 1995, pp. 703–709.

[11]Youngblood, J. W., Talay, T. A., and Pegg, R. J., "Design of Long-Endurance Unmanned Airplanes Incorporating Solar and Fuel Cell Propulsion," AIAA Paper 84-1430, June 1984.

[12]Harmats, M., "High Altitude, Long Endurance RPV with Hybrid Propulsion—Feasibility Study," M.S. Thesis, Technion—Israel Inst. of Technology, Haifa, Israel, Sept. 1996.

[13]Bryson, A. E., and Ho, Y. C., *Applied Optimal Control*, Ginn and Co., Boston, MA, 1969.

[14]Adkins, C. N., and Liebeck, R. H., "Design of Optimum Propellers," AIAA Paper 83-0190, Jan. 1983.

[15]Heyson, H. H., Riebe, G. D., and Fulton, C. L., "Theoretical Parametric Study of the Relative Advantages of Winglets and Wing-Tip Extensions," NASA TP 1020, Sept. 1977.

[16]Maughmer, M. D., and Somers, M., "Design and Experimental Results for a High Altitude, Long Endurance Airfoil," *Journal of Aircraft*, Vol. 26, No. 2, 1989, pp. 148–152.

[17]McLaughlin, M. D., "Calculations and Comparison with an Ideal Minimum of Trimmed Drag for Conventional and Canard Configurations Having Various Levels of Static Stability," NASA TN D-8391, May 1977.

[18]McCormick, B. W., *Aerodynamics, Aeronautics and Flight Mechanics*, Wiley, New York, 1979.

[19]Wilkinson, R. E., and Benway, R. B., "Liquid-Cooled Turbocharged Propulsion System for HALE Application," American Society of Mechanical Engineers, Paper 91-GT-399, June 1991.

[20]Anderson, W., "An Advanced Electric Drivetrain for EVs," *10th International Electric Vehicle Symposium* (Hong Kong), Society of Automotive Engineers, Warrendale, PA, 1990, pp. 209–221.

[21]Nicolai, L. M., *Fundamentals of Aircraft Design*, Univ. of Dayton, Dayton, OH, 1984.

[22]Martin, R. E., Garow, J., and Michaels, K. B., "Regenerative Fuel Cell Energy Storage System for a Low Earth Orbit Space Station," NASA CR-174802, Aug. 1984.

[23]Bolwin, K., "Application of Regenerative Fuel Cells for Space Energy Storage: A Comparison to Battery Systems," *Journal of Power Sources*, Vol. 40, July 1992, pp. 307–321.

[24]Raymer, D. P., *Aircraft Design—A Conceptual Approach*," AIAA Education Series, AIAA, Washington, DC, 1992.

[25]Johnstone, R., and Arntz, N., "Condor—High Altitude Long Endurance (HALE) Automatically Piloted Vehicle (APV)," AIAA Paper 90-3279, Sept. 1990.

[26]Hoerner S. F., *Fluid–Dynamic Drag*, Hoerner Fluid Dynamics, Brick Town, NJ, 1965.

[27]Wilkinson, R. E., "Design and Development of the Voyager 200/300 Liquid Cooled Aircraft Engine," Society of Automotive Engineers, Paper 871042, April 1987.

[28]Patterson C., "Unmanned High Altitude Long—Endurance Aircraft," AIAA Paper 89-2011, July 1989.

[29]Venkayya, V. B., and Tischler, V. A., "High Altitude Long—Endurance Aircraft Design Studies," *AGARD Meeting on Recent Advances in Long Range and Long Endurance Operation of Aircraft*, NATO, Brussels, Belgium, 1993, pp. 1–17.

[30]Strganac, T. W., "Wind Study for High Altitude Platform Design," NASA RP1044, Oct. 1979.